Near-field analysis of metallic DFB lasers at telecom wavelengths

L. Greusard,[1] D. Costantini,[2] A. Bousseksou,[2] J. Decobert,[3] F. Lelarge,[3] G.-H. Duan,[3] Y. De Wilde,[1,*] and R. Colombelli[2,4]

[1]*Institut Langevin, CNRS UMR7587, 1, rue Jussieu, 75005 Paris, France*
[2]*Institut d'Electronique Fondamentale, Univ. Paris Sud, CNRS UMR8622, 91405 Orsay, France*
[3]*III-V Lab, Joint lab of 'Alcatel-Lucent Bell Labs France, 'Thales Research and Technology' and 'CEA Leti', route de Nozay, 91461 Marcoussis cedex, France*
[4]*raffaele.colombelli@u-psud.fr*
** yannick.dewilde@espci.fr*

Abstract: We image in near-field the transverse modes of semiconductor distributed feedback (DFB) lasers operating at λ ≈1.3 μm and employing metallic gratings. The active region is based on tensile-strained InGaAlAs quantum wells emitting transverse magnetic polarized light and is coupled via an extremely thin cladding to a nano-patterned gold grating integrated on the device surface. Single mode emission is achieved, which tunes with the grating periodicity. The near-field measurements confirm laser operation on the fundamental transverse mode. Furthermore – together with a laser threshold reduction observed in the DFB lasers – it suggests that the patterning of the top metal contact can be a strategy to reduce the high plasmonic losses in this kind of systems.

OCIS codes: (140.5960) Semiconductor lasers; (230.5750) Resonators; (240.6680) Surface plasmons.

References and links

1. J. J. Coleman, A. C. Bryce, and C. Jagadish, *Advances in Semiconductor Lasers* (Academy, 2012).
2. J. Carroll, J. Whiteaway, and D. Plumb, *Distributed Feedback Semiconductor Lasers* (The Institution of Electrical Engineers IEE, 1998), Vol. 86.
3. W. Zeller, L. Naehle, P. Fuchs, F. Gerschuetz, L. Hildebrandt, and J. Koeth, "DFB lasers between 760 nm and 16 μm for sensing applications," Sensors (Basel Switzerland) **10**(4), 2492–2510 (2010).
4. J. Singh, *Semiconductor Optoelectronics* (McGraw-Hill, 1995), pp. 527.
5. M. Kamp, J. Hofmann, F. Schäfer, M. Reinhard, M. Fischer, T. Bleuel, J. P. Reithmaier, and A. Forchel, "Lateral coupling: a material independent way to complex coupled DFB lasers," Opt. Mater. **17**(1-2), 19–25 (2001).
6. W. Kaiser, K. Mathwig, S. Deubert, J. P. Reithmaier, A. Forchel, O. Parillaud, M. Krakowski, D. Hadass, V. Mikhelashvili, and G. Eisenstein, "Static and dynamic properties of laterally coupled DFB lasers based on InAs/InP QDash structures," Electron. Lett. **41**(14), 808–810 (2005).
7. M. Kamp, J. Hofmann, A. Forchel, F. Schäfer, and J. P. Reithmaier, "Low-threshold high-quantum efficiency laterally gain-coupled InGaAs/AlGaAs distributed feedback lasers," Appl. Phys. Lett. **74**(4), 483–485 (1999).
8. A. Bousseksou, Y. Chassagneux, J. R. Coudevylle, R. Colombelli, C. Sirtori, G. Patriarche, G. Beaudoin, and I. Sagnes, "Surface-plasmon distributed-feedback quantum cascade lasers operating pulsed, room temperature," Appl. Phys. Lett. **95**(9), 091105 (2009).
9. M. Carras and A. De Rossi, "Photonic modes of metallodielectric periodic waveguides in the mid-infrared spectral range," Phys. Rev. B **74**(23), 235120 (2006).
10. A. Bousseksou, R. Colombelli, A. Babuty, Y. De Wilde, Y. Chassagneux, C. Sirtori, G. Patriarche, G. Beaudoin, and I. Sagnes, "A semiconductor laser device for the generation of surface-plasmons upon electrical injection," Opt. Express **17**(11), 9391–9400 (2009).
11. R. Bachelot, G. Wurtz, and P. Royer, "An application of the apertureless scanning near-field optical microscopy: Imaging a GaAlAs laser diode in operation," Appl. Phys. Lett. **73**(23), 3333–3335 (1998).
12. G. Wurtz, R. Bachelot, and P. Royer, "Imaging a GaAlAs laser diode in operation using apertureless scanning near-field optical microscopy," Eur. Phys. J. Appl. Phys. **5**(3), 269–275 (1999).
13. N. Yu, L. Diehl, E. Cubukcu, C. Pflügl, D. Bour, S. Corzine, J. Zhu, G. Höfler, K. B. Crozier, and F. Capasso, "Near-field imaging of quantum cascade laser transverse modes," Opt. Express **15**(20), 13227–13235 (2007).
14. N. Yu, L. Diehl, E. Cubukcu, D. Bour, S. Corzine, G. Höfler, A. K. Wojcik, K. B. Crozier, A. Belyanin, F. Capasso, and F. Capasso, "Coherent coupling of multiple transverse modes in quantum cascade lasers," Phys. Rev. Lett. **102**(1), 013901 (2009).

#184092 - $15.00 USD Received 23 Jan 2013; revised 17 Apr 2013; accepted 17 Apr 2013; published 22 Apr 2013

15. R. Hillenbrand, B. Knoll, and F. Keilmann, "Pure optical contrast in scattering-type scanning near-field microscopy," J. Microsc. **202**(1), 77–83 (2001).
16. D. Costantini, L. Greusard, A. Bousseksou, Y. De Wilde, B. Habert, F. Marquier, J.-J. Greffet, F. Lelarge, J. Decobert, G.-H. Duan, and R. Colombelli, "A hybrid plasmonic semiconductor laser," Appl. Phys. Lett. **102**(10), 101106 (2013).
17. J. Decobert, N. Lagay, C. Cuisin, B. Dagens, B. Thedrez, and F. Laruelle, "MOVPE growth of AlGaInAs–InP highly tensile-strained MQWs for 1.3 mm low threshold lasers," J. Cryst. Growth **272**(1-4), 543–548 (2004).
18. D. Costantini, A. Bousseksou, M. Fevrier, B. Dagens, and R. Colombelli, "Loss and gain measurements of tensile-strained quantum well diode lasers for plasmonic devices at telecom wavelengths," IEEE J. Quantum Electron. **48**(1), 73–78 (2012).
19. D. Costantini, L. Greusard, A. Bousseksou, R. Rungsawang, T. P. Zhang, S. Callard, J. Decobert, F. Lelarge, G.-H. Duan, Y. De Wilde, and R. Colombelli, "In situ generation of surface plasmon polaritons using a near-infrared laser diode," Nano Lett. **12**(9), 4693–4697 (2012).
20. Comsol Multyphysics, www.comsol.com. The simulation is performed in 3D on a single period of the DFB cavity (p = 200nm) imposing Bloch periodic boundary conditions along the propagation direction.

1. Introduction

Semiconductor lasers have become essential tools for fiber-optic communications, optical sensing and photonics [1, 2]. Their compactness, efficiency and wide range of wavelengths are key features of this success. The implementation of a distributed feedback (DFB) resonator enhances their performances, allowing a precise control of the emission frequency and a reduction of the threshold current [3]. DFBs are typically realized by periodically structuring the semiconductor cladding close to the laser active region (AR) [4], or by adding a laterally coupled metallic grating [5–7]. In the latter case, which suits well devices operating in transverse electric (TE) polarization, a metallic grating is implemented laterally to a ridge laser: it couples evanescently with the laser guided modes, thus yielding a complex-coupled DFB laser. Epitaxial re-growth is no more needed in this case. An alternative strategy – which suits lasers operating in transverse magnetic (TM) polarization - consists in patterning the device top metal electrode into a 1st-order metal grating. No re-growth is needed in this case too. This approach was validated at long mid-infrared wavelengths (λ = 7.5 μm) [8]. In this region of the electromagnetic (EM) spectrum, the metallic ohmic losses are relatively low [9], and the long wavelength requires only a micron-sized lithography. These were significant advantages for a first validation of this concept [10]. In the mid-infrared, it was also shown that patterning the metallic layer leads to the onset of an extremely low-loss mode. The extension of this concept to the near-IR would be of importance, also because it would provide a possible strategy to overcome the huge ohmic losses in plasmonic systems *via* metal patterning. In the long term, it could also provide an alternative strategy for DFB devices, of course only if the metallic losses can be substantially reduced.

In this paper, we apply the aforementioned concept of metallic DFB to diode lasers operating at telecom wavelengths ($\lambda \approx 1.3$ μm) and in TM polarization. To demonstrate the metal grating effect, we also provide a direct imaging of the electromagnetic near-field at the laser facet *via* near-field scanning optical microscopy (NSOM). We employ an original method of aperture NSOM, which allows an excellent imaging quality free of background, even in the luminescence regime. Scattering NSOM is also effective to achieve such mappings [11–15], provided that extreme care is taken to avoid interferences due to stray far-field radiation.

We first present the device design and the fabrication details. We then illustrate the NSOM analysis results of the laser facet imaging, which leads to the unequivocal identification of the laser mode. Its field distribution analysis also allows us to elucidate the action of the metallic patterning.

2. Device design and fabrication

The laser design we have developed for this study is inspired from long mid-infrared quantum-cascade laser (QCL) devices ($\lambda \approx 7.5$ μm) featuring a 1st order metal grating patterned on the top metal electrode [8,10]. The transverse magnetic (TM) polarized light emitted by the QCL couples with the grating and gives rise to a low-loss hybrid plasmonic

#184092 - $15.00 USD Received 23 Jan 2013; revised 17 Apr 2013; accepted 17 Apr 2013; published 22 Apr 2013

mode. The electromagnetic energy density is then maximal on the active region, and not at the metal-semiconductor interface, as it would be the case for regular surface plasmon modes.

The present device operating at telecom wavelength is in essence very different from the QCL laser devices in Ref [8]. The shorter operating wavelength implies a dramatic increase of the ohmic losses, and a reduction of the grating period by a factor ~6 requires the use of high-resolution nano-lithography techniques.

Furthermore, while for QCL devices the active region is directly in contact with the DFB metallic grating, laser diodes are bipolar devices which need both p- and n-type charge reservoirs. Hence the diode active region is separated from the DFB metal grating by a p-doped, dielectric cladding layer. A metallic grating with a 100% duty cycle (continuous metal layer) results in a mode profile which is completely different in the two devices. While for QCLs the mode is a surface plasmon with intensity maximum at the metal-AR interface, the laser diode features a waveguide mode centered on the active region, with some coupling to a surface plasmon at the metal-cladding interface [9,10,16]. This peculiarity leads to significantly different behaviors of the modal losses as a function of the grating duty cycle, as discussed in the body of the paper.

Finally, QCLs naturally emit TM polarized light, while laser diodes in general operate on TE modes. This problem is circumvented by using tensile-strained InGaAlAs quantum wells to produce TM polarized light at $\lambda \approx 1.3$ μm [17–19].

Edge-emitting laser diodes based on interband transitions – in contrast with QCLs – can emit both TM and TE (transverse electric) polarized light, but they mostly operate in TE polarization. However, TM polarized emission at telecom wavelengths can be obtained using semiconductor ARs based on tensile-strained InGaAlAs quantum wells [17], which also provide elevated differential gains [18]. In the present work this same AR is separated from the metal-grating by an extremely thin (only 250 nm) InP upper cladding. It is constituted of a 100-nm-thick highly p-doped contact layer (unavoidable for efficient charge injection), a 100-nm-thick p-doped InP layer, and a 50-nm-thick non-intentionally-doped InP layer. A structure with an extremely thin cladding layer permits to experimentally elucidate the interaction of gain and metal, paving the way to the realization of efficient SPP generators [19] and – in perspective - semiconductor-based SPASERs.

The devices were processed into 9-μm-wide, 250-nm-deep mesa ridges. The surface was previously patterned with metal using electron-beam lithography followed by lift-off (Fig. 1(a)). The 1st-order grating has a periodicity of ≈200 nm for a duty cycle (DC) of ~50%. Its thickness (Ti/Au, 3/77 nm) has been chosen thicker than the skin depth at $\lambda = 1.3$ μm. An insulating layer of SiN was deposited by PECVD (plasma-enhanced chemical-vapor deposition) and then opened in correspondence of the top device surface to expose the metal grating. Side-metallic contacts were finally deposited (by evaporation followed by lift-off) for electrical contact purposes. Note: the width of the opening affects the functionality of the DFB laser. Figure 1 highlights that the SiN opening must be as wide as possible to avoid the onset of undesired lateral lobes.

#184092 - $15.00 USD Received 23 Jan 2013; revised 17 Apr 2013; accepted 17 Apr 2013; published 22 Apr 2013

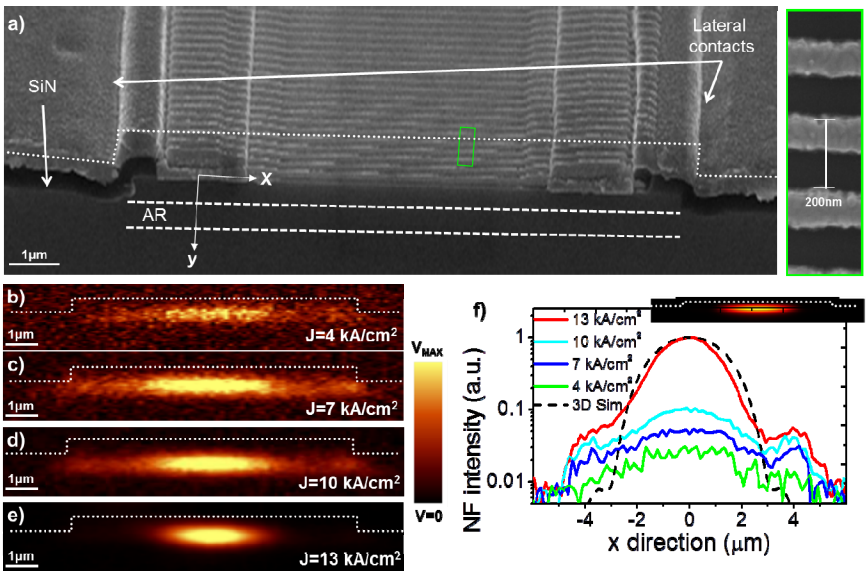

Fig. 1. a) Scanning electronic microscope (SEM) image of the DFB laser facet. The ridge width is 9 µm. The inset shows a small area of the device top surface containing three periods of the metal grating. b, c, d, e) NSOM images and simulation of the DFB laser facet showing the transversal mode electromagnetic field distribution at different operating currents of the device. (b) Measurement far below threshold, at an injected current density of J = 4 kA/cm^2 (color bar, V_{MAX} = 0.07V). (c) Measurement far below threshold, at an injected current density of J = 7 kA/cm^2 (color bar, V_{MAX} = 0.12V).(d) Measurement at threshold, at J = 10 kA/cm^2 (color bar, V_{MAX} = 0.24V). (e) Laser regime, at J = 13 kA/cm^2 (color bar, V_{MAX} = 2.25V).f) Horizontal cross-section (along the x-direction shown in (a)) of the NSOM measurements plotted in solid colored curves. The experimental cross-section of the laser mode in (f), corresponding to the red solid line, is to be compared with the horizontal cross-sections of the simulated mode in the inset, black dashed line. Inset: Plot of the squared electric field obtained from a 3D finite element simulation. The lowest loss mode is the fundamental one, with a maximum of the electric field under the metal fingers of the grating. The squared electric field in the x-y plane is plotted.

3. NSOM measurements and data interpretation

We have observed the EM near-field distribution of the laser mode by scanning the facets of the devices with a commercial NSOM (WITec GmbH alpha300S) which we have adapted to operate at near-infrared frequencies. A square hollow pyramid probe is mounted at the extremity of the cantilever of an atomic force microscope (AFM). The pyramid is made of aluminum, with a nano-aperture implemented at its apex (diameter ~100 nm). The device is mounted with its emitting facet oriented towards the objective of an optical microscope, and the pyramid is kept in permanent contact with the laser facet using an electronic feedback. The photons transmitted through the nano-aperture are collected by the microscope objective and focused into an optical fiber connected to a thermoelectrically-cooled InGaAs detector. The use of a hollow probe allows a very effective suppression of the far-field radiation from the laser facet, which would otherwise saturate the detector.

Figures 1(b)-1(e) show room temperature near-field measurements of the device facet, at injected current densities of 4, 7, 10 and 13 kA/cm^2. Images (b) and (c) were recorded below threshold, (d) at threshold, and (e) in the laser regime. The white-dotted lines materialize the edges of the ridge. Below threshold (Fig. 1(b) and 1(c)) we mainly detect the device luminescence which originates from the whole active region. In contrast, when the laser regime is established (Fig. 1(e)), we detect a single lobe which is well confined at the center of the ridge resonator and in the AR layer. The progressive transition from the luminescence

#184092 - $15.00 USD Received 23 Jan 2013; revised 17 Apr 2013; accepted 17 Apr 2013; published 22 Apr 2013

to the laser regime is visible in the strong confinement of the mode lobe upon increase of the injected current.

Figure 1(f) reports 1D transverse cross-sections – along the x-direction – of the NSOM measurements. The logarithmic scale highlights the transition from spontaneous to stimulated emission. Below the laser threshold, the NSOM detects a diffused luminescence signal along the ridge width, not negligible compared to the central maximum, and increasing with the injected current. Whereas above threshold (J>10 kA/cm^2,) the luminescence signal is clamped and the central lobe has a Gaussian shape. The black dotted line in Fig. 1(f) is a numerical simulation [20] (see also inset) which is in good agreement with the experiment, if the spontaneous emission component on the sides is neglected.

Note: the lateral contacts necessary to achieve electrical injection into the grating are continuous stripes which cover the patterned metal. The presence of this continuous metallic region at the resonator sides increases the optical losses for higher order transverse modes. The single-lobed fundamental mode emerges as the favored one for lasing.

4. Spectral analysis of the device

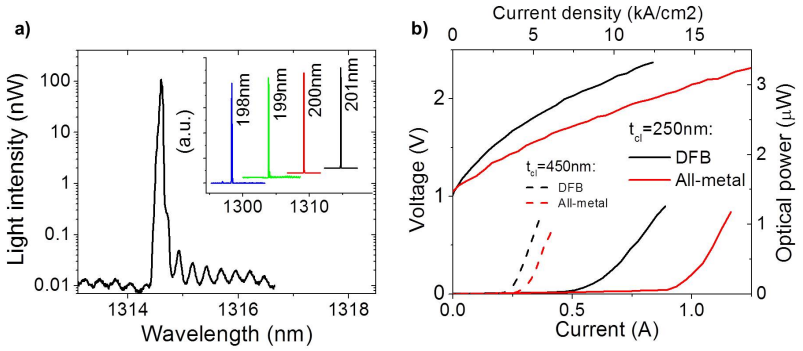

Fig. 2. a) Single mode spectra of a DFB laser with a grating periodicity of 201 nm, operating at J = 13kA/cm^2. The SMSR is more than 30 dB. The spectra were recorded by using a cleaved multimode optical fiber which is coupled to an optical spectrum analyzer b) Typical Light-Current-Voltage (LIV) characteristics of a DFB laser (black solid curves) and an all-metal laser, equivalent to a DFB laser with a duty cycle of 100% (red solid curves). Therefore the measured output powers are not representative of the total device output. The DFB device exhibits a larger differential resistance, but it presents a threshold reduction of more than 5 kA/cm^2 compared to the all-metal laser. Note: the DFB laser differential resistance is slightly larger than the one of the laser with full metallization (≈1 Ohm). The non uniformity of the top contact, due to the metal patterning, affects the current injection increasing the total resistance. The dashed lines are the light output power of a DFB laser (black dashed curve) and an all-metal laser (red dashed curve) fabricated on a structure with the same active region but with a cladding 200 nm thicker. In this case the threshold reduction of the DFB laser compared to the all-metal laser is of only 0.5 kA/cm^2.

Figure 2(a) shows the typical room-temperature (RT) emission spectrum of a 750-μm-long DFB laser with a grating periodicity p of 201 nm. Stable single mode emission at λ≈1300 nm with a side mode suppression ratio (SMSR) of more than 30 dB is obtained. The measured full width at half maximum is of about 8 GHz (0.05 nm).

The emission spectra were measured for different grating periods: 198, 199, 200 and 201 nm. Figure 2(a) shows that all the devices are single-mode. The emission correctly tunes with the periodicity of the grating, from λ = 1298 nm (p = 198 nm) up to λ = 1314 nm (p = 201 nm).

5. Comparison with an un-patterned laser

The peculiar properties of the DFB laser mode (DC ≈50%) can be best appreciated in comparison with a laser with an un-patterned top contact layer (equivalent to a DFB laser with

#184092 - $15.00 USD Received 23 Jan 2013; revised 17 Apr 2013; accepted 17 Apr 2013; published 22 Apr 2013

DC = 100%). The corresponding simulated field distributions are plotted in Figs. 3(a) and 3(b). The insets on the left show the 1D vertical cross-section of the squared electric field along the dotted lines. The cross-section of the 100% DC device shows two maxima, one located at the AR, and the other one at the interface between the dielectric cladding and the metal layer. The DFB laser exhibits instead a single maximum at the AR, similarly to a dielectric confined mode, and no field is present at the metal-semiconductor interface. Indeed the metal patterning effectively repels the field into the active region. This behavior is analogous to the one observed in mid-infrared QC lasers with metallic DFB gratings [10]. The simulated field distributions are in agreement with experimental NSOM measurements of the facets, which are shown in Fig. 3(c).

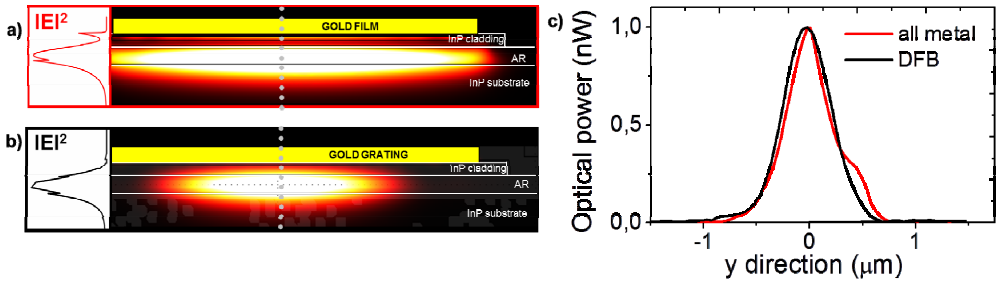

Fig. 3. a, b) Plot of squared electric field of a facet simulation and inset containing a vertical cross-section for a mode of: (a) A fully metallic cavity. To note the presence of the mode field in the AR and at the interface of the metal. (b) A DFB cavity. The mode shows instead a single maximum, located in the AR. c) Normalized experimental cross-section along the vertical direction (y-direction, where the zero corresponds to the center of the AR), for the mode of the all-metal cavity (red line) and the mode of the DFB cavity (black line).

The different field distribution between the fully metallic and the DFB laser entails a difference in optical losses and consequently a difference in laser threshold. We observed a reduction of the threshold current density (J_{th}) due to the metal patterning. Both devices can operate at RT in pulsed regime (Fig. 2(b)). The DFB J_{th} is ≈8 kA/cm^2, while the fully-plasmonic laser – whose emission is of course multimode - operates at ≈14 kA/cm^2, i.e. a threshold reduction of ≈40%.

The dashed curves in Fig. 2(b) correspond to the light-current characteristics of a fully metallic and a DFB device realized with the same active region, but with a 200 nm thicker InP cladding [15] (total cladding thickness of 450 nm). Since the metal is farther from the AR, threshold values are lower than the previous case. However, even in this case a slight threshold reduction of approximately 0.5 kA/cm^2 can be observed. The reduction is only of 15% because the grating is less coupled to the optical mode.

6. Calculations on the loss reduction

Finite element simulations provide a qualitative understanding of the loss reduction induced the metal patterning. The simulations are realized in 2D, but are compatible with the 3D simulations of Fig. 1(f) (inset) and Figs. 3(a) and 3(b). The calculation is performed by solving the 2D Helmholtz equation in a single unit cell. A similar analysis is reported in [10], but here - because of the presence of a thin top cladding - three different modes a priori exist, all satisfying the requirement of TM polarization and confinement in the AR larger than 30% [9].

The optical losses of the three modes as function of the DC (with a step of 0.2%) are plotted in Fig. 4(a). The field distributions of the low-loss mode (red dots) and of the high-loss mode DC<60% (blue squares) are depicted in Figs. 4(b) and 4(c). The field distributions corroborate the origin of the losses: the field overlaps with the metal. At around DC = 60% the losses of two modes diverge because in both cases the electric field is pulled toward the

#184092 - $15.00 USD Received 23 Jan 2013; revised 17 Apr 2013; accepted 17 Apr 2013; published 22 Apr 2013

metal and the confinement in the AR becomes less than 30%. This behavior is a typical feature of structures with a thin top cladding, as was shown in [9].

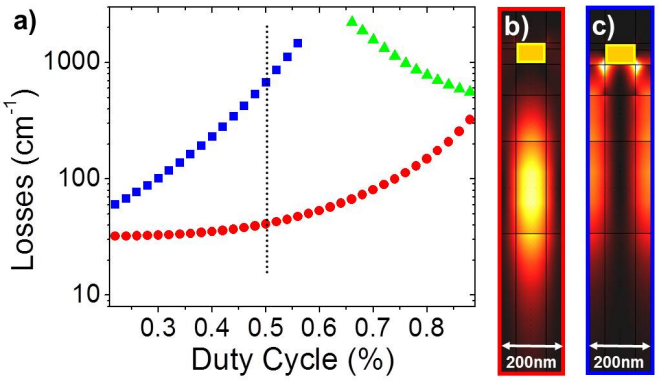

Fig. 4. a) Results of the 2D finite element simulations showing the modal losses as a function of the duty cycle of the DFB grating. We selected the modes which are TM polarized and have an active region (AR) confinement factor of more than 30%. At DC≈60% the two high-loss modes diverge and the AR confinement factor decreases. This behavior - not observed in Ref [10]. – is in fact typical of DFB lasers with a cladding layer between the AR and the metallic grating [9]. b, c) Longitudinal finite element simulation of a DFB laser period. The squared electric field is plotted for: (b) low-loss mode (red dots in panel a). The electric field is located *under* the metallic fingers and has no consistent overlap with the metal. This is in agreement with the NSOM measurements in Fig. 1(e). c) high-loss mode (blue squares in panel a). The electric field is located under the air slits, *between* the metallic fingers, and has a consistent overlap with the metal.

On the contrary, the low-loss mode never has a significant overlap with the metal, hence it is relatively independent of the grating DC. The DFB laser is expected to operate on this latter mode (Fig. 4(b)), as experimentally verified by the NSOM measurement (Fig. 1(e)).

While the operation on the low-loss mode is experimentally confirmed, the finite element simulations predict optical losses of ≈40 cm^{-1}, implying a J_{th} of ≈2 kA/cm^2 [18]. This value is much lower than the experimentally measured J_{th} (≈9 kA/cm^2), and the same holds for the thicker structure which should exhibit an even lower J_{th}. There are several possible reasons. The higher differential resistance exhibited by the DFB device entails more heating by Joule effect and a consequent lower efficiency. Furthermore, the electrical injection in correspondence of the grating – which serves also as top metal contact - is not as efficient as in presence of a continuous metal layer. The DFB device might experience a better current injection under the lateral strips (where a continuous metallization is present), and a worse current injection in the device core, where the laser mode is confined.

7. Conclusions

We have demonstrated a DFB laser device operating in single mode at telecom wavelengths (λ≈1.3 μm) with a metal grating extremely close to the active region. The near-field imaging of the facets is completely stray-light free and it provides experimental evidence of the operation on the fundamental, low-loss grating mode. NSOM results are in excellent agreement with the 3D finite element simulations. Moreover the comparison with a reference device shows a threshold reduction when the top metal is patterned. The device performances are not state of the art yet for laser diode technology (the J_{th} are very high), in particular compared to the efficient laterally coupled DFB lasers in Refs [5–7]. This very initial experimental evidence is noteworthy in the context of plasmonics, and for TM (not TE) diode lasers. In the very long term, perspective are present for device physics too, if the problem of non-perfect electrical injection is solved, and if the extreme loss reduction predicted by Fig. 4

#184092 - $15.00 USD Received 23 Jan 2013; revised 17 Apr 2013; accepted 17 Apr 2013; published 22 Apr 2013

is validated. Only in this case it will be possible to efficiently combine a simple metallic grating technology with TM polarized diode laser devices.

Acknowledgments

We thank Oliver Gauthier-Lafaye and Xavier Letartre for useful discussions. The device fabrication has been performed at the nano-center CTU-IEF-Minerve. This work was supported by the French National Research Agency (ANR-09-NANO-020 "GOSPEL", ANR-10-BLAN-1002 "CALIN") and from the Triangle de la Physique (Project "PHLARE"). This work is supported by LABEX WIFI (Laboratory of Excellence within the French Program "Investments for the Future") under reference ANR-10-IDEX-0001-02 PSL*. L.G. acknowledges support from the Direction Générale de l'Armement (DGA).

#184092 - $15.00 USD Received 23 Jan 2013; revised 17 Apr 2013; accepted 17 Apr 2013; published 22 Apr 2013